Journal of
Materials Chemistry C

PAPER

View Article Online
View Journal | View Issue

Cite this: *J. Mater. Chem. C*, 2024, **12**, 8398

Smart emissive hybrid dynamer and nanocomposite made of complementary organic and inorganic emitters combined *via* a supramolecular Janus synthon†

Ilya V. Kashnik,[ab] Jeanne Rebours,[a] Noée Dumait,[a] Konstantin A. Brylev [b] and Yann Molard *[a]

Received 15th March 2024,
Accepted 8th May 2024

DOI: 10.1039/d4tc01043d

rsc.li/materials-c

Monotopic and ditopic blue-emitting anthracene derivatives bearing one or two thymine moieties, respectively, are associated *via* hydrogen bonds to a red-emitting $[Mo_6I_8(OCOC_2F_5)_6]^{2-}$ anion, whose charge is counter-balanced by a Janus-type organic synthon made of an imidazolium head bearing an organic chain terminated with a complementary diamidopyridine group. The generated supramolecular hydrogen-bonded complex and dynamers show blue emission in solution and red emission in the solid state. Once embedded in the PMMA film, the dynamer emission colour is controlled by the irradiation time and power in the UV-2A region. This dynamic luminescent behaviour allows for evanescent optical writing on the film.

Introduction

Organic–inorganic materials are versatile substances whose abilities depend on the intrinsic properties of the isolated components and cooperative effects induced by their interactions. Depending on their functionalities, they show great potential in a tremendous number of fields such as housing, health and diagnosis, electronics, energy, and optics.[1,2] In particular, emissive responsive materials able to react to one or several external stimuli such thermal treatment, electrical or mechanical stress, chemical or vapor exposure, and light irradiation,[3–7] have been used in applications such as sensors, lighting, optoelectronics, data recording and storage, security and anti-counterfeiting.[8–10] In this regard, using supramolecular self-assembly to construct hybrid materials facilitates the structural control of molecular functionalities *via* a bottom-up process. Such a strategy, which enters in the paradigm of supramolecular material nanoarchitectonics,[11,12] can be used to design hybrid dynamers. Hybrid dynamers are supramolecular polymers, generated by the association of organic and inorganic monomers bearing complementary binding groups able to connect through reversible non-covalent interactions.[13,14]

In this work, we describe the generation of a supramolecular polymer *via* the recognition-controlled polyassociation of ditopic heterocomplementary blue- and red-emitting monomers.

While the blue emitter contains a well-known anthracene central core functionalized with two thymine moieties, the red emitter is a dianionic octahedral molybdenum nanocluster. The dynamic assembly between both emitters relies on a Janus-type organic linker made of a diamidopyridine moiety on one side and an imidazolium cationic head on the other.

Anthracene is an attractive building block owing to its ease of functionalization and efficient deep-blue emission with a high photoluminescence quantum efficiency.[15–18] It has been widely used in the design of photocyclizable supramolecular receptors for organic and inorganic guests,[19–22] blue organic light-emitting diodes (OLEDs),[23] and emissive moisture sensors[24] and was combined with various inorganic phosphors, among which $CsCu_2I_3$[25] or $CsPb(Br/I)_3$[26] nanocrystals are used to design white light-emitting diodes. However, in the solid state, π–π stacking between two anthracene units generally leads to a red shift and a strong quenching of its fluorescence due to excimer formation. This problem can be partially resolved by inhibiting π–π stacking through functionalization.

Octahedral molybdenum cluster complexes with the general formula $[Mo_6L^i_8L^a_6]^{2-}$ (L^i = inner ligand and L^a = apical ligand, see Scheme 1) are nanoscale inorganic building blocks obtained first through a high-temperature solid state chemistry route. The metallic Mo_6 scaffold is maintained by direct metal–metal bonds, covalently bonded to eight face-capping ligands

[a] *Université de Rennes, CNRS, ISCR – UMR 6226, SnMAT – UAR 2025, Rennes F-35000, France. E-mail: yann.molard@univ-rennes*
[b] *Nikolaev Institute of Inorganic Chemistry SB RAS, 3 Acad. Lavrentiev ave., 630090 Novosibirsk, Russian Federation*

† Electronic supplementary information (ESI) available. See DOI: **https://doi.org/10.1039/d4tc01043d**

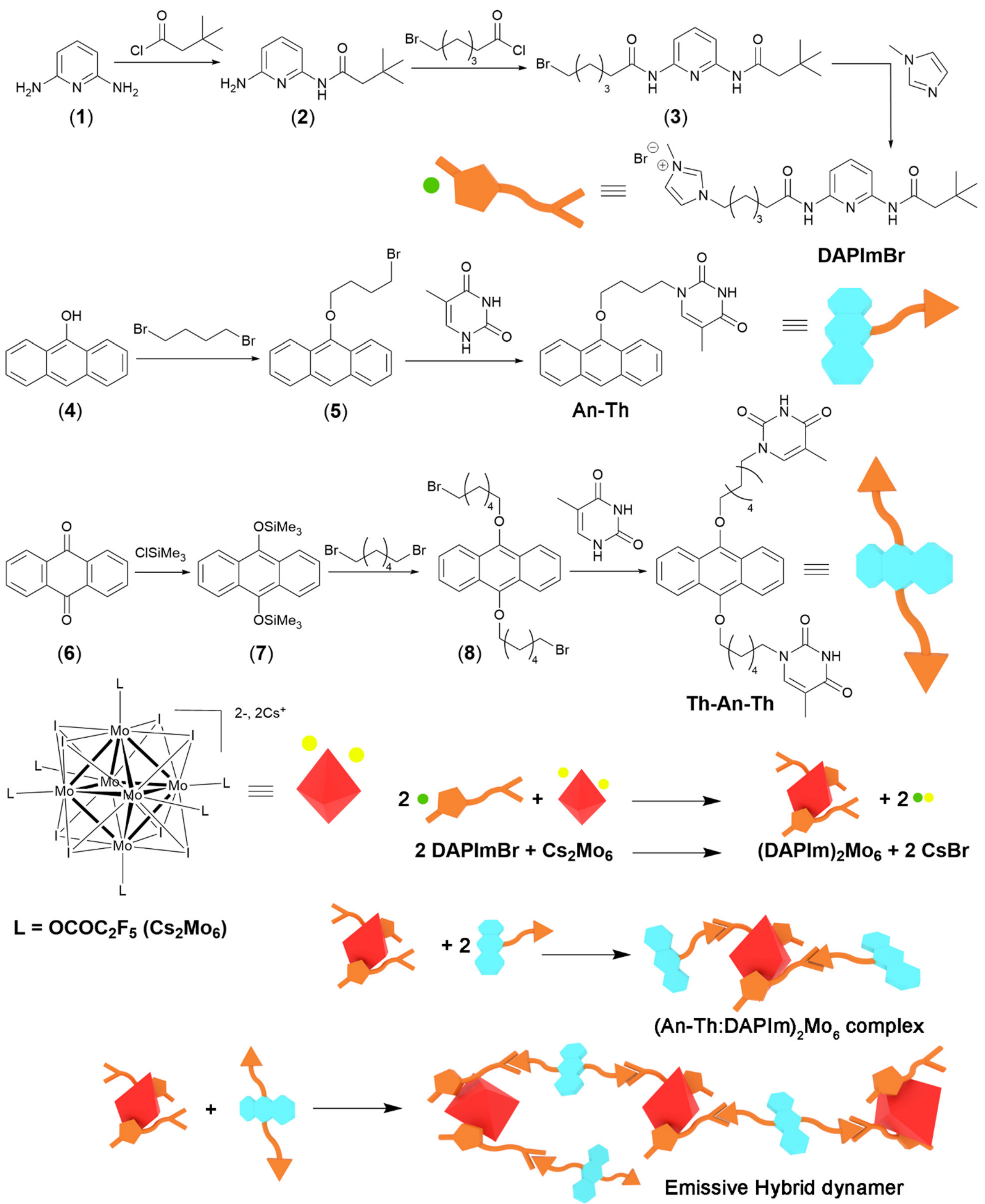

Scheme 1 Synthetic scheme of **DAPImBr** salt, monotopic **Th-An** and ditopic **Th-An-Th** ligands, functionalised cluster complex **(DAPIm)$_2$Mo$_6$**, emissive complex and hybrid dynamer containing complementary emitters.

(μ_3-L^i) and stabilized by six apical ligands (L^a).[27,28] Depending on the nature of inner and apical ligands, octahedral molybdenum cluster compounds can be highly red-NIR phosphorescent[29–31] with a very large Stokes shift[32] and show excellent photostability.[33,34] So far, they have been integrated in soft nanocomposites without the modification of their emission abilities,[35–38] thanks to their mainly metal-centred emission properties. In this work, we decided to use the $Cs_2[Mo_6I_8(OCOC_2F_5)_6]$ compound[33] as the starting material because it represents one of the most emissive and stable cluster complex described to date in the literature.[39–41]

Usually, dual-emissive materials are able to efficiently deliver a tailored emission that depends on the concentration and ratio of dyes. However, the degree of interactions between the emitters should also be considered to adjust the emission response toward the applied stimulus. As demonstrated herein, such an adjustment can be performed by introducing a hybrid dynamer in a host matrix, leading to a smart emissive nanocomposite whose emission colour is dependent on the irradiation time and power.

Results and discussion

Synthesis

As depicted in Scheme 1, the **DAPImBr** salt is a Janus-type organic linker. It bears an imidazolium head that will interact electrostatically with the dianionic cluster complex $[Mo_6I_8(OCOC_2F_5)_6]^{2-}$ (**Mo$_6$**) on one side, and on the other side, with a diamidopyridine moiety that possesses three complementary hydrogen-bond sites of thymine derivatives. It additionally bears a *tert*-butyl group to enhance its solubility in non-protic solvents.

DAPImBr was obtained in three steps starting from 2,6-diaminopyridine (**1**) by amide bond formation using first 3,3-dimethylbutyryl chloride to afford compound **2** and then 6-bromohexanoyl chloride to give compound **3**. Such reactions were performed in dry THF and in the presence of triethylamine. The intermediates were purified by column chromatography on silica gel. The reaction of **3** with *N*-methyl imidazole in $CHCl_3$ and a catalytic amount of I_2 led to the formation of the desired organic salt **DAPImBr**. The monotopic **An-Th** compound was mainly chosen as a model compound to study the supramolecular interactions between the thymine derivatives and **DAPImBr** or **(DAPIm)$_2$Mo$_6$**. It was synthesized in two steps starting from commercially available anthrone (**4**) that reacted with a large excess of 1,4-dibromobutane to afford compound **5**. The alkylation of thymine was then performed with **5** in DMSO at 25 °C under argon. The ditopic **Th-An-Th** was obtained in several steps: first, the reduction of 9,10-anthraquinone (**6**) with magnesium powder at reflux in THF under argon and in the presence of chlorotrimethylsilane, giving **7**, which was required prior to the reaction with 1,6-dibromohexane. **7** was isolated and crystallized as 9,10-dihydroxyanthracene.[22] **Th-An-Th** was then obtained by reacting **8** with a large excess of thymine. This compound shows a relatively poor solubility in non-polar solvents.

Targeted organic compounds were characterized by usual techniques such as ^{1}H and ^{13}C NMR (see ESI† Fig. S1–S13), mass spectrometry and elemental analysis. The Mo$_6$ cluster compound was functionalized with **DAPIm$^+$** cation quantitatively *via* a cationic metathesis to give **(DAPIm)$_2$[Mo$_6$I$_8$(OCOC$_2$F$_5$)$_6$]** (further labelled as **(DAPIm)$_2$Mo$_6$**). The purity of this hybrid building block was assessed by EDS (no traces of Br or Cs) and by elemental analysis. The ^{1}H NMR studies in $CDCl_3$ indicate that associating **DAPIm$^+$** with the **Mo$_6$** anion induces an increase in the electron density on the imidazolium ring, which is reduced by an upfield shift of the imidazolium protons signals from 10.26, 7.46 and 7.32 ppm down to 9.18, 7.35 and 7.26 ppm (see ESI† Fig. S16).

Complexes were obtained in solution by mixing **(DAPIm)$_2$Mo$_6$** with **An-Th** or **Th-An-Th** in a 2 : 1 or 1 : 1 stoichiometric ratio, respectively, followed by solvent evaporation. Due to the weakness and plurality of soft interactions, no single crystal suitable for structural determination could be obtained. Hence, spectroscopic methods were used to get insights into the assembling behaviour.

Binding studies

DAPIm$^+$ and thymine-containing anthracene derivatives possess hydrogen bond binding sites, allowing the formation of triply hydrogen-bonded complementary pairs that should lead for **Th-An-Th** to the formation of supramolecular polymers known as dynamers. The association of such units is well described in the literature,[42–46] and the calculated binding constant are generally lower than 1000 M^{-1},[21] which makes ^{1}H NMR spectroscopy the most suited spectroscopic method to evaluate them.[47] Hence, we first investigated the behaviour of **DAPImBr** in $CDCl_3$ upon the addition of aliquots of a $CDCl_3$ solution containing **An-Th**, and, to get insight into the influence of the Mo$_6$ cluster, we performed the same study with **(DAPIm)$_2$Mo$_6$**. The ^{1}H NMR spectra area of interest are reproduced in Fig. 1a for the titration involving the bromide salt, and Fig. 1b presents the plots of amide proton signal positions for **DAPImBr** and **(DAPIm)$_2$Mo$_6$** against the number of **An-Th** equivalents added to the deuterated solutions (see ESI† Tables S1, S2 and Fig. S17 for all other titration data). In both cases, the sequential addition of **An-Th** solution aliquots leads to a downfield shift of the two amide proton signals belonging to **DAPIm$^+$** from 8.32 and 8.98 ppm to 9.77 and 9.98 ppm, respectively. Meanwhile, the NH proton signal of thymine shows an upfield shift from 8.77 to 8.57 ppm. These results are a clear indication of the formation of the complementary hydrogen-bonded pairs in solution. From these titration curves, binding constant values of $K_a = 261 \pm 2$ M^{-1} and $K_a = 420 \pm 3$ M^{-1} were deduced for **An-Th:DAPImBr** and **(An-Th:DAPIm)$_2$Mo$_6$** complexes, respectively.[47] Such values are in the expected range for supramolecular systems based on triple hydrogen-bonded pairs and demonstrate a poor influence of the cluster core on the hydrogen-bonded assemblies. This is also expected considering the size of the linker between the imidazolium head and the diamido pyridine moiety.

The dynamer formation between **Th-An-Th** and **(DAPIm)$_2$Mo$_6$** could also be evidenced by looking at the upfield shift from 8.88 down to 8.46 ppm of the amine proton signals belonging to the thymine moieties upon increasing the **Th-An-Th** concentration in a solution of **(DAPIm)$_2$Mo$_6$** (see ESI† Fig. S18). However, considering that **Th-An-Th** started to crystallize at concentration higher than about 10^{-4} M in aprotic deuterated solvent, its poor solubility prohibited the calculation of the binding constant. Considering that the monotopic and ditopic ligands are made of the same building blocks, we can reasonably assume that

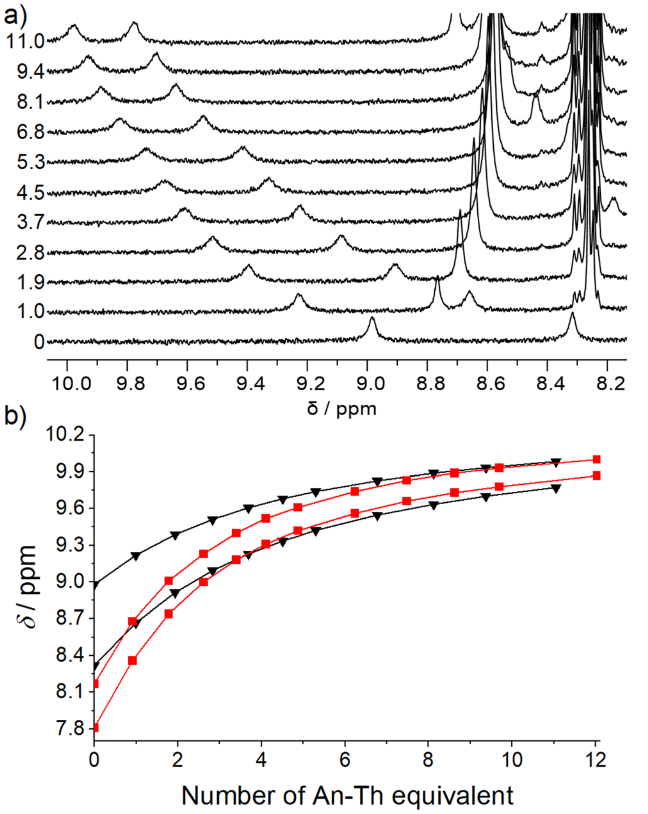

Fig. 1 (a) Evolution of the ^{1}H NMR spectrum of **DAPImBr** in $CDCl_3$ ([**DAPImBr**] = 9.86 × 10^{-4} M) upon the addition of **An-Th**; (b) follow up of the chemical shift of amide protons *vs.* [**An-Th**]/[**DAPIm+**] in $CDCl_3$ (black triangles for titration with **DAPImBr**; red squares for titration with **(DAPIm)$_2$Mo$_6$**).

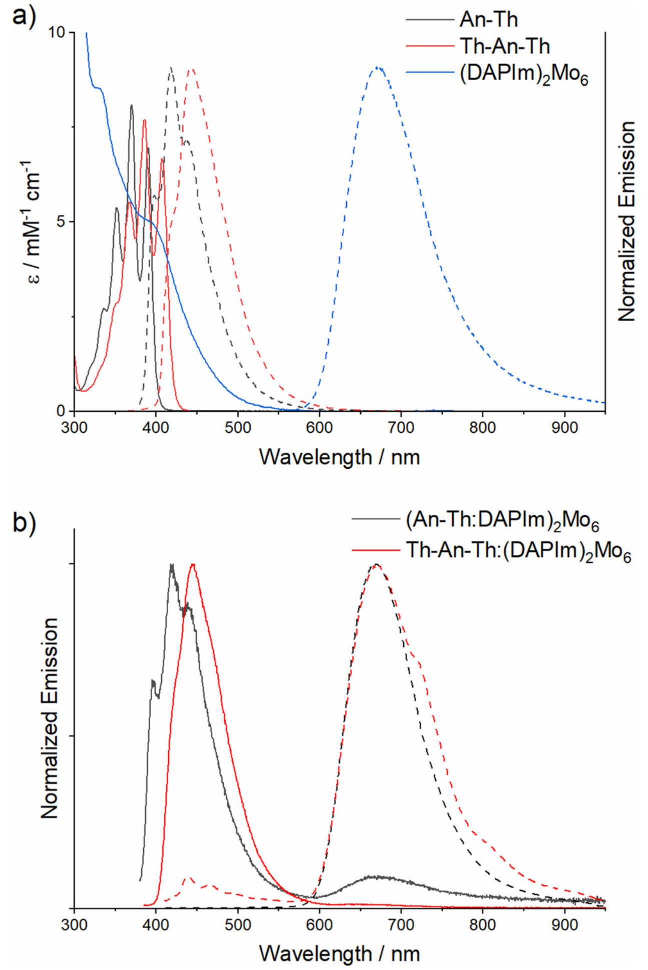

Fig. 2 (a) Absorption spectra (plain lines) and emission spectra (λ_{exc} = 375 nm, dashed lines) in CH_3CN of **An-Th** (black), **Th-An-Th** (red) and **(DAPIm)$_2$Mo$_6$** (blue); (b) emission spectra (λ_{exc} = 375 nm) of **(An-Th:DAPIm)$_2$Mo$_6$** (black) and **Th-An-Th:(DAPIm)$_2$Mo$_6$** (red) in $CHCl_3$ (plain lines) and in the solid state (dashed lines).

interactions between **Th-An-Th** and **DAPIm$^+$** should be of the same strength than with the previous system.

Absorption and emission studies

The absorption spectra of **An-Th** and **Th-An-Th** recorded in CH_3CN show the typical signature of the anthracene ^1L_a absorption band between 300 and 420 nm (Fig. 2a), while the **(DAPIm)$_2$Mo$_6$** spectrum presents the typical absorption band of the $\{Mo_6I_8\}^{4+}$ cluster core in the UV area and up to 500 nm, together with the absorption band of diamido pyridine centred at about 293 nm.

At this stage, we wish to state that thymine derivatives are well known to undergo a reversible photocyclization under UV-irradiation at their absorption maximum wavelength, which stands at about 280 nm.[48–50] In our case, the excitation wavelength will always be at a much lower energy (375–450 nm), which precludes the formation of thymine photodimers.

The addition of 1 equivalent of **An-Th** in a CH_3CN **DAPImBr** or **(DAPIm)$_2$Mo$_6$** solution does not induce a shift of the diamido pyridine absorption band, which is a typical behaviour for host:guest systems with low binding constant values.[20,21] At higher **An-Th** concentration, the overlap between the thymine and the diamidopyridine absorption bands precludes any clear conclusion about a shift appearance (see ESI† Fig. S19 and S20).

Steady state and time-dependent emission studies were realized in solution and in the solid state. Fig. 2 presents the emission spectra observed for **An-Th**, **Th-An-Th**, **(DAPIm)$_2$Mo$_6$**, and the corresponding mixtures, while all the recorded photophysical data are gathered in Table 1 (see ESI† Fig. S21–S31 for emission decay and fits). **An-Th** and **Th-An-Th** exhibit the typical cyan broad emission of anthracene in solution in its monomeric form with emission maxima at 422 and 443 nm, respectively. Emission lifetime decay could be fitted with one component, confirming the monomeric nature of the anthracene emission (no interactions between anthracene moieties in solution) with lifetime values of 5.7 and 13.4 ns for **An-Th** and **Th-An-Th**, respectively. Their emission in the solid state differs largely: while the same emission envelope is observed for **An-Th**, **Th-An-Th** shows a red-shifted and broader emission envelope that is attributed to anthracene excimer formation, as observed previously in the literature (see ESI† Fig. S32).[21] The emission signal of the hexamolybdenum cluster anion is not sensitive to the nature of its counter cation nor to the complex

Table 1 Photophysical data recorded in solution, in the solid state and in PMMA at λ_{exc} = 375 nm: emission maxima (λ_{max}), excited states lifetime (τ_i) with corresponding amplitude (a_i), average lifetime (τ_{av}) and absolute quantum yield in air (Φ)

Compound	λ_{max}, nm	τ_1 (a_1, %)	τ_2 (a_2, %)	τ_3 (a_3, %)	τ_{av}	Φ, %
An-Th[a]	422	5.7 ns	—	—	5.7 ns	44
An-Th[b]	422	8.5 ns (1)	1.5 ns (14)	0.4 ns (85)	1.7 ns	3
Th-An-Th[a]	443	13.4 ns	—	—	13.4 ns	60
Th-An-Th[b]	455	15 ns (6)	5.8 ns (18)	1.0 ns (76)	7.5 ns	17
$(DAPIm)_2Mo_6$[a]	670	63 μs (69)	36 μs (31)	—	57 μs	32
$(DAPIm)_2Mo_6$[b]	670	39 μs (49)	18 μs (51)	—	32 μs	12
$(An\text{-}Th{:}DAPIm)_2Mo_6$[b]	668	70 μs (42)	33 μs (58)	—	55 μs	6
$Th\text{-}An\text{-}Th{:}(DAPIm)_2Mo_6$[bc]	668	158 μs (9)	69 μs (36)	17 μs (55)	84 μs	1
Pol_{An}	440	17 ns	—	—	17 ns	97
Pol_{Mo}	668	111 μs (45)	53 μs (55)	—	90 μs	12
Pol_{dyn}	440	11 ns (63)	3.4 ns (37)	—	9.8 ns	10 47[d]
	668	124 μs (7)	38 μs (93)	—	55 μs	
Pol_{dyn}[c]	440	10 ns (48)	3.4 ns (52)	—	8.2 ns	—
	668	243 μs (73)	123 μs (27)	—	224 μs	—

[a] In solution. [b] In the solid state. [c] Lifetime measured in vacuum. [d] After 1 minute under UV-2A irradiation. Average lifetime is calculated as $\tau_{av} = \left(\Sigma a_i \tau_i^2\right)/(\Sigma a_i \tau_i)$.

formation with anthracene-based compounds. A broad emission centred at 670 nm is always observed either in deaerated solution (as all phosphorescent species, Mo_6 emissive derivatives are subject to O_2 quenching) or in the solid state (see ESI† Fig. S33).

The overlap between the anthracene emission band and the Mo_6 cluster anion absorption band leads to a very efficient energy transfer. Indeed, the calculated Förster distance for this system is 5.85 nm (see ESI† Fig. S34). The efficiency of this energy transfer was verified in a $CHCl_3$ solution by a titration experiment involving the stepwise increase of **$(DAPIm)_2Mo_6$** concentration while keeping the **An-Th** concentration constant. Each addition of the cluster complex led to the partial quenching of **An-Th**, whose emission disappeared completely after the addition of 14 equivalents of **$(DAPIm)_2Mo_6$** (see ESI† Table S4 and Fig. S35). The nature of this energy transfer seems to be of trivial type (resonance energy transfer), as confirmed by evaluating the anthracene moiety excited state lifetime value that remained unchanged (around 6 ns) upon the addition of up to 3 equivalents of **$(DAPIm)_2Mo_6$** (see ESI† Table S3 and Fig. S36–S39).

Fig. 2b presents the emission spectra recorded in solution and in the solid state for hybrid supramolecular complexes **$(An\text{-}Th{:}DAPIm)_2Mo_6$** and **$Th\text{-}An\text{-}Th{:}(DAPIm)_2Mo_6$**. They were prepared by mixing stoichiometric amounts of **DAP_2Mo** and **An-Th** or **Th-An-Th** in $CHCl_3$ in 1 : 2 or 1 : 1 ratio, respectively, and then evaporating to dryness. In aerated solution, the anthracene emission band is more intense, while deaerating the solution leads to the increase of the cluster emission band. In the solid state, however, only the red emission of the cluster component is observed with an enhancement of its average lifetime compared to **DAP_2Mo** from 32 μs to 55 μs. These facts actually indicate the efficient energy transfer from the anthracene to the cluster complex.

The dynamer was also let under constant irradiation at 375 nm to check its stability, and we observed an enhancement of the cluster emission band by about 14% after the first 20 seconds of irradiation, which was followed by a slight decrease.

Design of a smart emissive nanocomposite

Considering that in the solid state only the emission band of **$(DAPIm)_2Mo_6$** is observed in the overall emission signal envelope of pure **$Th\text{-}An\text{-}Th{:}(DAPIm)_2Mo_6$** dynamer, we decided to lower the supramolecular interactions strength between the emitters by embedding the dynamer in a poly(methylmetacrylate) (PMMA) matrix. We hypothesized that such an embedment would affect the inter-emitters distance and lead to the enhancement of the anthracene emission band by lowering the energy transfer efficiency to the cluster compound. Considering that PMMA has a high degree of rigidity compared to other host matrices and a triplet energy of 3.1 eV,[51] this is a suitable wide band gap host matrix and a material of choice to observe luminescence from our emitters.[52]

Hence, a homogeneous 2.3 wt%-doped PMMA film was obtained by the slow evaporation of the $CHCl_3$/MeOH (8 : 1) mixture containing commercial PMMA and the dynamer (**Pol_{dyn}**). For the sake of comparison, PMMA samples containing either **$(DAPIm)_2Mo_6$** (**Pol_{Mo}**) or **Th-An-Th** (**Pol_{An}**) at the same concentration than in **Pol_{dyn}** were also prepared. The samples are presented in Fig. 3a under day light and UV-2A irradiation, while the emission spectra at the beginning of the irradiation are presented in Fig. 3b. According to its emission spectrum and calculated excited state lifetime, **Th-An-Th** behaves in the PMMA film like in solution. Only the bifunctionalized anthracene monomer emission is recorded with an excitation decay that could be fitted with a 17 ns single component. In the presence of **$(DAPIm)_2Mo_6$**, the **Th-An-Th** emission decay was fitted with two components with an average lifetime value of 9.8 or 8.2 ns in air or in vacuum, respectively. Such a decrease is attributed to the remaining energy transfer from the organic emitter to the inorganic one.

As presented in Fig. 3c, a prolonged excitation of **Pol_{dyn}** at 375 nm, with the pulsed laser diode used for lifetime studies, leads to the enhancement of the cluster compound emission band and a slight lowering of the anthracene one. The ratio value between the two emission maxima intensity I_{668}/I_{440} passes from 0.9 to 2.8 after 10 s and stabilizes around 3 after

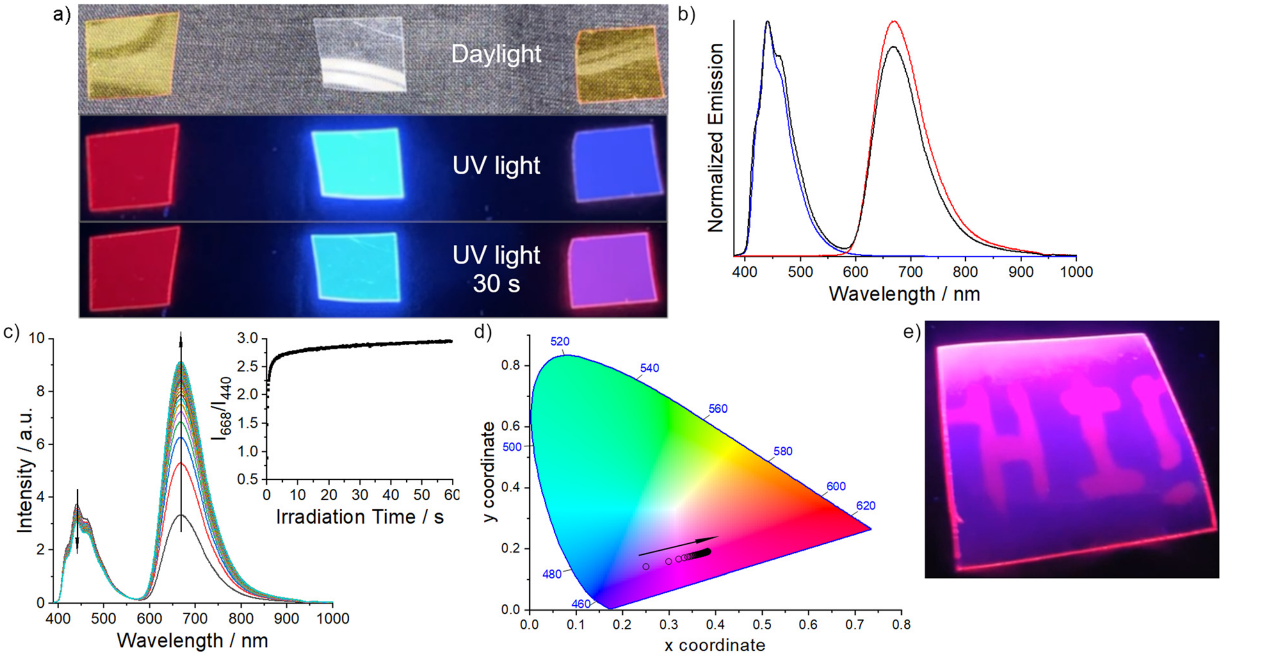

Fig. 3 (a) Doped PMMA films under daylight and UV-2A irradiation immediately after turning on the UV lamp and after 30 s (left: $\mathbf{Pol_{Mo}}$, center: $\mathbf{Pol_{An}}$, right: $\mathbf{Pol_{dyn}}$); (b) emission spectra recorded for $\mathbf{Pol_{An}}$ (blue), $\mathbf{Pol_{Mo}}$ (red) and $\mathbf{Pol_{dyn}}$ (black); (c) evolution of the emission envelop of $\mathbf{Pol_{dyn}}$ film under 1 min irradiation at 375 nm in air (inset: follow up of the emission maxima intensity ratio with the irradiation time); (d) 1931 CIE coordinates diagram for 1 min irradiation at 375 nm; (e) $\mathbf{Pol_{dyn}}$ film exposed under UV-2A after the optical writing up of "Hi!" with a 405 nm laser pointer.

1 min of irradiation. Therefore, the emission colour of the dynamer containing film depends on the irradiation time and power and passes from blue (CIE coordinates: $x = 0.25$, $y = 0.14$) to red (CIE coordinates: $x = 0.38$, $y = 0.19$) upon irradiation (Fig. 3d). Moreover, the irradiation also affects the absolute quantum yield, which goes from 0.10 to 0.47 after 1 min under a 4 W UV-2A lamp. Keeping the sample in the dark leads to the recovery of the blue emission colour. Such behaviour allowed us to use $\mathbf{P_{dyn}}$ as a support for optical writing with a 5 mW 405 nm laser pointer, as depicted in Fig. 3e (see also ESI† Video S1 for the writing process). The mechanism of the colour changes, and thus the writing process, is attributed to the increase of the cluster compound emission efficiency induced by a depletion of the local O_2 concentration within the PMMA film upon irradiation. We already observed such a phenomenon when $[Mo_6I_8(OCOC_2F_5)_6]^{2-}$ was associated with oxindole[53] or tetraphenylethylene[54] derivatives. In fact, the O_2 concentration lowering is induced by the reaction of the fundamental O_2 ($^3\Sigma_g^-$) triplet state with the cluster compound excited triplet state. The O_2 consumption rate is related to the cluster compound excited state generation, which explains why irradiation time and power are deeply related to stabilize the cluster emission. Indeed, when the dynamer-doped PMMA film is placed under high vacuum (1.9×10^{-6} hPa), the intensity of the blue and red components does not vary with a I_{668}/I_{440} ratio value of 10.3 upon constant irradiation even after 300 s (see ESI† Fig. S40).

Experimental

Starting materials were purchased from Alfa Aesar or Aldrich and used without any further purification. All solvents were distilled and dried before use. $Cs_2[Mo_6I_8(OCOC_2F_5)_6]$ precursor was obtained by the reported procedures.[33] NMR experiments were realized at 298 K on a Bruker AV III 400 MHz spectrometer fitted with a BBFO probe and Bruker AV III HD 500 MHz spectrometer fitted with a BBFO probe. All peaks were referenced to the methyl signals of TMS at δ = 0 ppm. Mass spectrometry and elemental analysis were performed with a Bruker MaXis 4G spectrometer and a Thermo Fisher Flash EA1112 microanalyzer, respectively, at the Centre Régional de Mesures Physiques de l'Ouest (CRMPO). UV-vis absorption spectra and excitation *vs.* emission maps were recorded with a Horiba Duetta spectrophotometer. The absolute quantum yields were measured with a C9920-03 Hamamatsu system. Lifetime measurements and TRPL mapping at 296 K were realized using a picosecond laser diode (Jobin Yvon deltadiode, 375 nm) and a Hamamatsu C10910-25 streak camera mounted with a slow single sweep unit. Signals were integrated on the whole emission decay. Fits were calculated using Hamamatsu software and the goodness of fit judge by the reduced χ^2 value and residual plot shape. Irradiation time-dependent emission studies were performed with the picosecond 375 nm laser diode used for lifetime measurements. Spectra were recorded with an Ocean Optics QEPro CCD spectrometer.

Synthetic procedures

***N*-(6-aminopyridin-2-yl)-3,3-dimethylbutanamide (2).** Compound **2** was synthesized according to the procedure reported by Dirksen *et al.*[55] 2,6-diaminopyridine (14.0 g, 128.3 mmol) was placed in a three-necked round bottom flask equipped with a magnetic stirrer and a dropping funnel. The air was removed and the system was filled with Ar. Dry THF (100 mL) and triethylamine (3.9 mL, 28 mmol) were added into the flask. 3,3-Dimethylbutyryl chloride (3.2 mL, 23 mmol) and dry THF (40 mL) were placed in the dropping funnel, and the solution was added dropwise into the flask at 0 °C. After full addition, the solution was stirred overnight at RT, the residue was filtered off, and the solvent was removed under reduced pressure. The product was dissolved in CH_2Cl_2 and washed with saturated $NaHCO_3$ aqueous solution. The organic phase was collected and dried over anhydrous $MgSO_4$, filtrated and the solvent was removed under reduced pressure. The product was purified by column chromatography on silica gel (CH_2Cl_2/ethyl acetate (4 : 1) as eluent). Then, the product was dried at 60 °C overnight under vacuum to give compound **2** as a white solid (3.7 g, 78%). ^1H NMR (400 MHz, $CDCl_3$) δ = 7.63 (s, 1H, NH), 7.58 (d, J = 8.0, 1H, CH_{py}–C–NH), 7.46 (t, J = 7.9, 1H, CH), 6.26 (d, J = 7.9, 1H, CH_{py}–C–NH_2), 4.32 (s, 2H, NH_2), 2.21 (s, 2H, CH_2), 1.09 (s, 9H, $3CH_3$). ^{13}C NMR (101 MHz, $CDCl_3$) δ = 170.21 (C=O), 157.05 (C_{py}), 149.83 (C_{py}), 140.12 (C_{py}), 104.18 (C_{py}), 103.26 (C_{py}), 51.72 (CH_2), 31.29 (C–$(CH_3)_3$), 29.80 ($3CH_3$). MS (ESI, CH_3OH/CH_2Cl_2 90/10): [M+H] $C_{11}H_{18}N_3O$ m/z (theoretical) = 208.1444, m/z (found) = 208.1448; [M+Na] $C_{11}H_{17}N_3ONa$ m/z (theoretical) = 230.1264, m/z (found) = 230.1266. E.A.: calc. for $C_{11}H_{17}N_3O$: C, 63.74; H, 8.27; N, 20.27; found: C, 63.87; H, 8.18; N, 19.97.

6-Bromo-*N*-(6-(3,3-dimethylbutanamido)pyridin-2-yl)hexanamide (3). Compound **2** (3.5 g, 16.9 mmol) was placed in a three-necked round bottom flask equipped with a magnetic stirrer and a dropping funnel. The air was removed and the system was filled with Ar. Dry THF (70 mL) and triethylamine (2.6 mL, 18.7 mmol) were added into the flask. 6-Bromohexanoyl chloride (3.2 mL, 20.9 mmol) and dry THF (40 mL) were placed in the dropping funnel, and the solution was added dropwise into the flask at 0 °C. After full addition, the solution was stirred overnight at RT, the residue was filtered off, and the solvent was removed under reduced pressure. The product was dissolved in CH_2Cl_2 and washed with saturated $NaHCO_3$ aqueous solution. The organic phase was collected and dried over anhydrous $MgSO_4$, filtrated and the solvent was removed under reduced pressure. The product was purified by column chromatography on silica gel (CH_2Cl_2/ethyl acetate (9 : 1) as eluent). Then, the product was dried at 60 °C overnight under vacuum to give compound **3** as a white solid (4.68 g, 72%). ^1H NMR (400 MHz, $CDCl_3$) δ = 7.91 (dd, J = 13.7, 8.1 Hz, 2H, $2CH_{py}$–C–NH), 7.71 (t, J = 8.1 Hz, 1H, CH_{py}), 7.65 (s, 1H, NH), 7.57 (s, 1H, NH), 3.43 (t, J = 6.7 Hz, 2H, CH_2–Br), 2.41 (t, J = 7.4 Hz, 2H, CH_2–C(O)NH), 2.25 (s, 2H, CH_2–C$(CH_3)_3$), 1.97–1.86 (m, 2H, CH_2), 1.82–1.70 (m, 2H, CH_2), 1.60–1.48 (m, 2H, CH_2), 1.11 (s, 9H, $3CH_3$). ^{13}C NMR (101 MHz, $CDCl_3$) δ = 171.05 (C=O), 170.25 (C=O), 149.42 (C_{py}), 149.35 (C_{py}), 140.86 (C_{py}), 109.44 (C_{py}), 109.41 (C_{py}), 51.75 (CH_2), 37.44 (CH_2), 33.46 (CH_2), 32.42 (CH_2), 31.36 (C–$(CH_3)_3$), 29.79 ($3CH_3$), 27.69 (CH_2), 24.36 (CH_2). MS (ESI, CH_3OH/CH_2Cl_2 90/10): [M+Na] $C_{17}H_{26}N_3O_2BrNa$ m/z (theoretical) = 406.11006, m/z (found) = 406.1110. [M+H] $C_{17}H_{27}N_3O_2Br$ m/z (theoretical) = 384.1281, m/z (found) = 384.1283. Traces: [M_2+Na] $C_{17}H_{26}N_3O_2ClNa$ m/z (theoretical) = 362.1606, m/z (found) = 362.1609. E.A.: calc. for $C_{17}H_{26}N_3O_2Br$: C, 53.13; H, 6.82; N, 10.93; found: C, 53.51; H, 6.64; N, 10.45.

1-(6-((3-(3,3-Dimethylbutanamido)phenyl)amino)-6-oxohexyl)-3-methyl-1*H*-imidazol-3-ium bromide (DAPImBr). To a solution of compound **3** (1 g, 2.6 mmol) in $CHCl_3$ (40 mL), 1-methylimidazole (0.25 mL, 3.1 mmol) and catalytic amount of I_2 were added. The solution was stirred under reflux for 48 h. Excess of pentane was added, and the solution was left for 30 h to yield a white powder. The powder was dried at 60 °C overnight under vacuum to give compound **DAPImBr** as a white solid (420 mg, 32%). ^1H NMR (400 MHz, $CDCl_3$) δ = 10.26 (s, 1H, $CH_{imidazole}$), 9.13 (s, 1H, NH), 8.54 (s, 1H, NH), 7.89 (d, J = 8.1 Hz, 1H, CH_{py}), 7.79 (d, J = 8.1 H, 1H, CH_{py}), 7.64 (t, J = 8.1 Hz, 1H, CH_{py}), 7.46 (s, 1H, $CH_{imidazole}$), 7.32 (s, 1H, $CH_{imidazole}$), 4.31 (t, J = 7.3 Hz, 2H, N–CH_2), 4.04 (s, 3H, N–CH_3), 2.54 (t, J = 7.3 Hz, 2H, CH_2), 2.28 (s, 2H, CH_2), 1.98 (p, J = 7.5 Hz, 4H, $2CH_2$), 1.75 (p, J = 7.4 Hz, 2H, CH_2), 1.41 (p, J = 7.6 Hz, 2H, CH_2), 1.07 (s, 9H, $3CH_3$). ^{13}C NMR (101 MHz, $CDCl_3$) δ = 172.23 (C=O), 171.14 (C=O), 149.88 (C_{py}), 140.45 (C_{py}), 137.58 (C_{py}), 123.12 ($C_{imidazole}$), 122.26 ($C_{imidazole}$), 109.40 (C_{py}), 109.34 (C_{py}), 51.03 (CH_2), 49.77 (CH_2), 36.72 ($C_{imidazole}$), 36.62 (CH_2), 31.35 (C–$(CH_3)_3$), 29.79 ($3CH_3$), 29.41 (CH_2), 25.10 (CH_2), 24.23(CH_2). MS (ESI, CH_3OH/CH_2Cl_2 90/10): [M+] $C_{21}H_{32}N_5O_2$ m/z (theoretical) = 386.2551, m/z (found) = 386.2548. E.A.: calc. for $C_{21}H_{32}N_5O_2Br\cdot0.25CHCl_3$: C, 51.43; H, 6.55; N, 14.11; found: C, 51.30; H, 6.82; N, 14.09. UV-vis in CH_3CN λ_{max}, nm (ε, mol^{-1} dm^3 cm^{-1}): 297 (12352), 293 sh (11570), 285 sh (9399), 261 (3548), 254 (3534).

9-(4-Bromobutoxy)anthracene (5). Compound **5** was synthesized according to the procedure reported by Wang *et al.*[56] 1,4-dibromobutane (9 mL, 74.6 mmol), K_2CO_3 (2.3 g, 16.6 mmol) and acetone (150 mL) were placed in a two-necked round bottom flask equipped with a condenser and protected with Al foil. The solution was deaerated with Ar and anthrone (3 g, 15 mmol) was added. The mixture was stirred at reflux under Ar atmosphere for 14 h. The residue was filtered off, and the solvent was removed under reduced pressure. The product was dissolved in CH_2Cl_2 and washed with saturated NaCl aqueous solution. The organic phase was collected and dried over anhydrous $MgSO_4$, filtrated and the solvent was removed under reduced pressure. The product was purified by column chromatography on silica gel (pentane/CH_2Cl_2 (9 : 1) as eluent). Then, the product was dried at 60 °C overnight under vacuum to give compound **5** as a white solid (1.82 g, 37%). ^1H NMR (400 MHz, $CDCl_3$) δ = 8.33–8.18 (m, 3H, $3CH_{anthracene}$), 8.06–7.99 (m, 2H, $2CH_{anthracene}$), 7.56–7.44 (m, 4H, $4CH_{anthracene}$), 4.26 (t, J = 6.2 Hz, 2H, O–CH_2), 3.64 (t, J = 6.5 Hz, 2H, Br–CH_2), 2.36 (dtd, J = 8.9, 6.7, 4.9 Hz, 2H, CH_2), 2.29–2.19 (m, 2H, CH_2). MS (ESI, CH_3OH/CH_2Cl_2 90/10): [M+H] $C_{18}H_{18}OBr$ m/z (theoretical) = 329.0535, m/z (found) = 329.0534; [M] $C_{18}H_{17}OBr$ m/z (theoretical) = 328.0457, m/z (found) = 328.0449. E.A.: calc. for $C_{18}H_{17}OBr$: C, 65.67; H, 5.20; found: C, 65.83; H, 4.99.

1-(4-(Anthracen-9-yloxy)butyl)-5-methylpyrimidine-2,4(1*H*,3*H*)-dione (An-Th). Thymine (2.7 g, 21.4 mmol), K_2CO_3 (0.6 g, 4.3 mmol) and DMSO (40 mL) were placed in a flask protected with Al foil. The solution was deaerated with Ar and compound **5** (0.5 g, 1.5 mmol) was added. The mixture was stirred at RT under

Ar atmosphere for 48 h. The residue was filtered off. H_2O was added to the solution to yield a mixture of thymine and product as a white powder. The product was dissolved in CH_2Cl_2 and thymine was filtered off. Excess of pentane was added to the solution and left for 3 h to yield a yellow powder. The powder was dried at 60 °C overnight under vacuum to give compound **An-Th** as a slightly yellow solid (240 mg, 40%). ^{1}H NMR (500 MHz, $CDCl_3$) δ = 8.87 (s, 1H, NH), 8.28–8.22 (m, 3H, $3CH_{anthracene}$), 8.06–7.96 (m, 2H, $2CH_{anthracene}$), 7.49 (dpd, J = 7.5, 6.2, 1.5, 4H, $4CH_{anthracene}$), 7.10 (q, J = 1.2, 1H, $CH_{thymine}$), 4.26 (t, J = 5.9, 2H, CH_2–O), 3.93 (t, J = 7.0, 2H, CH_2–N), 2.22–2.05 (m, 4H, $2CH_2$), 1.96 (d, J = 1.2, 3H, CH_3). ^{13}C NMR (126 MHz, $CDCl_3$) δ = 164.19 (NH–C=O), 150.89 (N–C=O/$C_{anthracene}$–O), 140.54 (N–CH), 132.43 ($C_{anthracene}$), 128.56 ($C_{anthracene}$), 125.53 ($C_{anthracene}$), 125.46 ($C_{anthracene}$), 125.33 ($C_{anthracene}$), 125.13 ($C_{anthracene}$), 124.61 ($C_{anthracene}$), 122.50 ($C_{anthracene}$), 122.35 ($C_{anthracene}$), 122.08 ($C_{anthracene}$), 110.77 (C–CH_3), 75.09 (CH_2–O), 48.64 (CH_2–N), 27.54 (CH_2–CH_2–O), 26.32 (CH_2–CH_2–N), 12.37 (CH_3). MS (ESI, CH_3OH/CH_2Cl_2 90/10): [M+Na] $C_{23}H_{22}N_2O_3Na$ m/z (theoretical) = 397.1523, m/z (found) = 397.1525; [M–H+2Na] $C_{23}H_{21}N_2O_3Na_2$ m/z (theoretical) = 419.1342, m/z (found) = 419.1342; [M+K] $C_{23}H_{22}N_2O_3K$ m/z (theoretical) = 413.1262, m/z (found) = 413.1260. E.A.: calc. for $C_{23}H_{22}N_2O_3$: C, 73.78; H, 5.92; N, 7.48; found: C, 73.77; H, 5.74; N, 7.36. UV-vis in CH_3CN λ_{max}, nm (ε, mol^{-1} dm^3 cm^{-1}): 390 (6967), 370 (8107), 352 (5375), 335 (2718), 320 sh (1202).

9,10-Bis((trimethylsilyl)oxy)anthracene (7). Compound **7** was synthesized according to the procedure reported by Marquis *et al.*[22] Anthraquinone (2 g, 10 mmol) and magnesium powder (480 mg, 20 mmol) were placed in a three-necked round bottom flask equipped with a condenser and protected with Al foil. Air was removed, the system was filled with Ar and dry THF (150 mL) was added. After the complete solubilization of anthraquinone, chlorotrimethylsilane (10.2 mL, 80 mmol) was added. Finally, dry DMSO (0.5 mL) was added dropwise, and the reaction mixture was kept under reflux for 2 h. After this amount of time, the solvent was removed under oxygen-free conditions and dry pentane (25 mL) was added. The resulting solution was filtered and left in a freezer for 15 h. Light green crystals formed inside. The crystals were collected and dried at 60 °C overnight to give compound **7** (2,45 g, 72%). ^{1}H NMR (400 MHz, $CDCl_3$) δ = 8.25–8.17 (m, 4H, $4CH_{anthracene}$), 7.48–7.40 (m, 4H, $4CH_{anthracene}$), 0.35 (s, 18H, $6CH_3$).

9,10-Bis((6-bromohexyl)oxy)anthracene (8). 1,6-Dibromohexane (17.5 mL, 113 mmol), K_2CO_3 (1.2 g, 8.5 mmol) and acetone (50 mL) were placed in a three-necked round-bottom flask equipped with a condenser, dropping funnel and protected with Al foil. The solution was deaerated with Ar. Compound **7** (1 g, 2.8 mmol) was dissolved in deaerated acetone (50 mL) and placed in the dropping funnel. The system was heated to reflux and compound **7** was added dropwise. After the full addition of compound **7**, the mixture was kept under reflux for 2 h. Then, the residue was filtered off, and the solvent was removed under reduced pressure. The product was purified by column chromatography on silica gel (first with pentane and then with pentane/Et_2O (49 : 1) as the eluent). Then, the product was dried at 60 °C overnight under vacuum to give compound **8** as a yellow-greenish solid (1 g, 66%). ^{1}H NMR (300 MHz, $CDCl_3$) δ = 8.33–8.25 (m, 4H, $4CH_{anthracene}$), 7.54–7.46 (m, 4H, $4CH_{anthracene}$), 4.19 (t, J = 6.5 Hz, 4H, $2CH_2$–O), 3.50 (t, J = 6.7 Hz, 4H, $2CH_2$–Br), 2.04 (ddt, J = 24.8, 14.1, 6.8 Hz, 8H, $4CH_2$), 1.83–1.59 (m, 8H, $4CH_2$). MS (ESI, CH_3OH/CH_2Cl_2 90/10): [M+H] $C_{26}H_{33}O_2Br_2$ m/z (theoretical) = 535.08418, m/z (found) = 535.0842; [M] $C_{26}H_{32}O_2Br_2$ m/z (theoretical) = 534.07635, m/z (found) = 534.0760; [M–HBr+H] $C_{26}H_{32}O_2Br$ m/z (theoretical) = 455.15802, m/z (found) = 455.1562. E.A.: calc. for $C_{26}H_{32}O_2Br_2$: C, 58.22; H, 6.01; found: C, 58.23; H, 6.03.

1,1′-((Anthracene-9,10-diylbis(oxy))bis(hexane-6,1-diyl))bis(5-methylpyrimidine-2,4(1*H*,3*H*)-dione) (Th-An-Th). Thymine (7.5 g, 60 mmol), K_2CO_3 (640 mg, 4.5 mmol) and DMSO (70 mL) were placed in a flask protected with Al foil. The solution was deaerated with Ar and compound **8** (800 mg, 1.5 mmol) was added. The mixture was stirred at RT under Ar atmosphere for 48 h. The residue was filtered off. H_2O was added to the solution to yield a mixture of thymine and product as a white powder. The product was dissolved in $CHCl_3$ and thymine was filtered off. Excess of pentane was added to the solution and left in a fridge to yield a yellowish crystalline powder. The powder was dried at 60 °C overnight under vacuum to give compound **Th-An-Th** as a slightly yellow solid (327 mg, 35%). ^{1}H NMR (400 MHz, MeOD) δ = 8.31–8.22 (m, 4H, $4CH_{anthracene}$), 7.54–7.48 (m, 4H, $4CH_{anthracene}$), 7.46 (d, J = 1.3 Hz, 2H, $2CH_{thymine}$), 4.17 (t, J = 6.4 Hz, 4H, $2CH_2$–O), 3.79 (t, J = 7.2 Hz, 4H, $2CH_2$–N), 2.06 (p, J = 6.6 Hz, 4H, $2CH_2$–CH_2–O), 1.87 (dd, J = 8.8, 1.2 Hz, 6H, $2CH_3$), 1.78 (ddd, J = 16.2, 12.4, 7.5 Hz, 8H, $4CH_2$), 1.60–1.48 (m, 4H, $2CH_2$). ^{13}C NMR (101 MHz, MeOD) δ = 165.48 (C=O), 151.60 (C=O), 147.14, 141.77 ($CH_{thymine}$), 125.02 ($CH_{anthracene}$), 122.18 ($CH_{anthracene}$), 109.72, 75.52 (CH_2–O), 47.90 (CH_2–N), 30.04 (CH_2–CH_2–O), 28.55 (CH_2), 26.01 (CH_2), 25.64 (CH_2), 10.74 (CH_3). MS (ESI, CH_3OH/CH_2Cl_2 90/10): [M+Na] $C_{36}H_{42}N_4O_6Na$ m/z (theoretical) = 649.29966, m/z (found) = 649.3002; [M+K] $C_{36}H_{42}N_4O_6K$ m/z (theoretical) = 665.27359, m/z (found) = 665.2736; [M–H+2Na] $C_{36}H_{41}N_4O_6Na_2$ m/z (theoretical) = 671.2816, m/z (found) = 671.2816; [M–H+Na+K] $C_{36}H_{41}N_4O_6NaK$ m/z (theoretical) = 687.25554, m/z (found) = 687.2554. E.A.: calc. for $C_{36}H_{42}N_4O_6$ + $0.5H_2O$: C, 68.01; H, 6.81; N, 8.81; found: C, 68.26; H, 6.70; N, 8.62. UV-vis in $CHCl_3$ λ_{max}, nm (ε, mol^{-1} dm^3 cm^{-1}): 407 (6670), 385 (7686), 367 (5531), 349 sh (2783), 332 sh (1153).

$(C_{21}H_{32}N_5O_2)_2[Mo_6I_8(OCOC_2F_5)_6]$ ((DAPIm)$_2$Mo$_6$). To a solution of $Cs_2[Mo_6I_8(OCOC_2F_5)_6]$ (0.5 g, 176 μmol) in acetone (10 mL), a solution of compound **DAPImBr** (165 mg, 354 μmol) in acetone (10 mL) was added. The resulting solution was stirred at 60 °C for 2 h. The solvent was removed under reduced pressure, the product was dissolved in CH_2Cl_2 and the residue was filtered off. The solvent was again removed under reduced pressure and the product was dried at 60 °C overnight under vacuum to give compound **(DAPIm)$_2$Mo$_6$** as an orange solid (550 mg, 93%). ^{1}H NMR (400 MHz, CD_2Cl_2) δ = 8.95 (s, 1H, $CH_{imidazole}$), 8.25 (s, 1H, NH), 7.96 (s, 1H, NH), 7.88 (d, J = 8.0 Hz, 1H, CH_{py}), 7.82 (d, J = 8.0 Hz, 1H, CH_{py}), 7.72

(t, J = 8.0 Hz, 1H, CH_{py}), 7.37 (dt, J = 22.1, 1.9 Hz, 2H, $2CH_{imidazole}$), 4.28 (t, J = 7.1 Hz, 2H, N–CH_2), 3.98 (s, 3H, N–CH_3), 2.47 (t, J = 7.0 Hz, 2H, CH_2–O), 2.27 (s, 2H, CH_2–C(CH_3)$_3$), 1.98 (p, J = 7.2 Hz, 2H, CH_2), 1.79 (p, J = 7.1 Hz, 2H, CH_2), 1.44 (p, J = 7.7 Hz, 2H, CH_2), 1.11 (s, 9H, $3CH_3$). ^{19}F NMR (376 MHz, CD_2Cl_2) δ = −82.54 (CF_3), −120.42 (CF_2). E.A.: calc. for $C_{60}H_{64}F_{30}I_8Mo_6N_{10}O_{16}$: C, 21.56; H, 1.93; N, 4.19; found: C, 21.23; H, 1.93; N, 4.12. EDS: Mo : I = 6.0 : 7.8 (no presence of Cs). UV-vis in CH_3CN λ_{max}, nm (ε, mol^{-1} dm^3 cm^{-1}): 406 sh (4538), 338 sh (8035), 289 (51036).

Preparation of supramolecular complexes

(An-Th:DAPIm)$_2$Mo$_6$: 50 mg (15 μmol) of **(DAPIm)$_2$Mo$_6$** and 11 mg (30 μmol) of compound **An-Th** were dissolved in 10 mL of $CHCl_3$. The solvent was removed under reduced pressure to yield an orange powder of **(An-Th:DAPIm)$_2$Mo$_6$**.

Th-An-Th:(DAPIm)$_2$Mo$_6$: 50 mg (15 μmol) of **(DAPIm)$_2$Mo$_6$** and 18.8 mg (30 μmol) of compound **Th-An-Th** were dissolved in 10 mL of $CHCl_3$. The solvent was removed under reduced pressure to yield an orange powder **Th-An-Th:(DAPIm)$_2$Mo$_6$**.

Preparation of doped PMMA films

All films were prepared using commercial PMMA (MW: 120 000 g mol^{-1}).

Pol$_{Mo}$: 2 g of PMMA and 40 mg of compound **(DAPIm)$_2$Mo$_6$** were dissolved in 30 mL of CH_2Cl_2. The resulting solution was placed in a closed Petri dish and left for evaporation at room conditions to yield a thin transparent orange film.

Pol$_{An}$: 2 g of PMMA and 7.5 mg of compound **Th-An-Th** were dissolved in 30 mL of CH_2Cl_2/MeOH mixture (8 : 1 v/v). The resulting solution was placed in a closed Petri dish and left for evaporation at room conditions to yield a thin transparent colorless film.

Pol$_{dyn}$: 2 g of PMMA, 40 mg of compound **(DAPIm)$_2$Mo$_6$** and 7.5 mg of compound **Th-An-Th** were dissolved in 30 mL of CH_2Cl_2/MeOH mixture (8 : 1 v/v). The resulting solution was placed in a closed Petri dish and left for evaporation at room conditions to yield a thin transparent orange film.

Conclusion

Supramolecular luminescent organic and inorganic building blocks bearing complementary hydrogen-bond binding group were synthesized. While blue-emitting anthracene derivatives were functionalized by one or two thymine groups, yielding the monotopic **An-Th** and ditopic **Th-An-Th** compounds, the red-NIR phosphorescent $[Mo_6I_8(OCOC_2F_5)_6]^{2-}$ cluster dianion was associated with two tailor-made organic Janus-type cations, *i.e.*, bearing an imidazolium head on one side to interact electrostatically with the inorganic anion and a diamidopyridine moiety on the other side to bind with the complementary thymine group of the blue emitter. The association constant deduced for **(An-Th:DAPIm)$_2$Mo$_6$** from the NMR titration experiment in $CDCl_3$ showed typical values for supramolecular assemblies based on triple hydrogen-bonded pair. Photophysical studies were first realized in solution and in the solid state and demonstrated an efficient energy transfer from the blue-emitting organic emitter to the red-NIR phosphorescent cluster to such an extent that only the cluster emission is observable. This behaviour was observed for both **(An-Th:DAPIm)$_2$Mo$_6$** supramolecular complex and **Th-An-Th:(DAPIm)2Mo6** dynamer. To minimize this energy transfer, the dynamer was embedded in an optically transparent PMMA matrix at 2 wt%. Such an integration increases the distance between the emitters by breaking the hydrogen-bonded network, thus leading to a blue-emitting polymer whose emission colour turns red under prolonged irradiation. This reversible emission colour change shows that the hybrid-doped PMMA film could serve as a medium for data encryption and reading, which would be performed using the same UV-2A light stimulus, a particularly efficient and cost-effective system for the end-user.

Author contributions

I. V. K: investigation, validation, writing – review – editing; J. R.: resources, writing – review – editing; N. D.: resources; K. A. B.: supervision, funding acquisition, writing – review – editing; Y. M.: conceptualization, investigation, funding acquisition, supervision, project administration, writing – original draft, writing – review & editing.

Conflicts of interest

There are no conflicts to declare.

Acknowledgements

Authors acknowledge Dr S. Cordier for financial support through the CLUSPOM IRP Network. I. V. K. thanks the French Embassy for providing the Vernadski scholarship for the co-tutelle PhD program between France and Russia. I. V. K. and K. A. B. thank Russian science foundation (project 19-73-20196-p). J. R. thanks the EUR LUMOMAT project and the Investments for the Future program ANR-18-EURE-0012 for PhD financial support.

References

1 C. Sanchez, P. Belleville, M. Popall and L. Nicole, *Chem. Soc. Rev.*, 2011, **40**, 696–753.
2 S. Parola, B. Julián-López, L. D. Carlos and C. Sanchez, *Adv. Funct. Mater.*, 2016, **26**, 6506–6544.
3 Y. Sagara and T. Kato, *Nat. Chem.*, 2009, **1**, 605–610.
4 S. Yamane, K. Tanabe, Y. Sagara and T. Kato, *Top. Curr. Chem.*, 2012, **318**, 395–406.
5 X. Ma and H. Tian, *Acc. Chem. Res.*, 2014, **47**, 1971–1981.
6 M.-K. Tsang, G. Bai and J. Hao, *Chem. Soc. Rev.*, 2015, **44**, 1585–1607.
7 E. Cariati, E. Lucenti, C. Botta, U. Giovanella, D. Marinotto and S. Righetto, *Coord. Chem. Rev.*, 2016, **306**, 566–614.

8 X. Yu, H. Chen, X. Shi, P.-A. Albouy, J. Guo, J. Hu and M.-H. Li, *Mater. Chem. Front.*, 2018, **2**, 2245–2253.
9 Y. Zhang, S. Zhou, K. C. Chong, S. Wang and B. Liu, *Mater. Chem. Front.*, 2019, **3**, 836–841.
10 P. Alam, N. L. C. Leung, Y. Cheng, H. Zhang, J. Liu, W. Wu, R. T. K. Kwok, J. W. Y. Lam, H. H. Y. Sung, I. D. Williams and B. Z. Tang, *Angew. Chem., Int. Ed.*, 2019, **58**, 4536–4540.
11 K. Ariga, M. Li, G. J. Richards and J. P. Hill, *J. Nanosci. Nanotechnol.*, 2011, **11**, 1–13.
12 M. Aono and K. Ariga, *Adv. Mater.*, 2016, **28**, 989–992.
13 J.-M. Lehn, *Prog. Polym. Sci.*, 2005, **30**, 814–831.
14 N. Roy, B. Bruchmann and J.-M. Lehn, *Chem. Soc. Rev.*, 2015, **44**, 3786–3807.
15 M. Yoshizawa and J. K. Klosterman, *Chem. Soc. Rev.*, 2014, **43**, 1885–1898.
16 G. S. Baviera and P. M. Donate, *Beilstein J. Org. Chem.*, 2021, **17**, 2028–2050.
17 H. Bouas-Laurent, A. Castellan, J. P. Desvergne and R. Lapouyade, *Chem. Soc. Rev.*, 2000, **29**, 43–55.
18 H. Bouas-Laurent, A. Castellan, J.-P. Desvergne and R. Lapouyade, *Chem. Soc. Rev.*, 2001, **30**, 248–263.
19 G. McSkimming, J. H. R. Tucker, H. Bouas-Laurent, J. P. Desvergne, S. J. Coles, M. B. Hursthouse and M. E. Light, *Chem. – Eur. J.*, 2002, **8**, 3331–3342.
20 Y. Molard, D. M. Bassani, J.-P. Desvergne, P. N. Horton, M. B. Hursthouse and J. H. R. Tucker, *Angew. Chem., Int. Ed.*, 2005, **44**, 1072–1075.
21 Y. Molard, D. M. Bassani, J.-P. Desvergne, N. Moran and J. H. R. Tucker, *J. Org. Chem.*, 2006, **71**, 8523–8531.
22 D. Marquis, J.-P. Desvergne and H. Bouas-Laurent, *J. Org. Chem.*, 1995, **60**, 7984–7996.
23 B. Chen, B. Liu, J. Zeng, H. Nie, Y. Xiong, J. Zou, H. Ning, Z. Wang, Z. Zhao and B. Z. Tang, *Adv. Funct. Mater.*, 2018, **28**, 1803369.
24 S. Miho, K. Imato and Y. Ooyama, *RSC Adv.*, 2022, **12**, 25687–25696.
25 W. Liu, K. W. Ng, H. Lin, Z. Dai, J. Xu, S. Su, Z. Tang and S. Wang, *J. Phys. Chem. C*, 2021, **125**, 13076–13083.
26 X. Shen, C. Sun, X. Bai, X. Zhang, Y. Wang, Y. Wang, H. Song and W. W. Yu, *ACS Appl. Mater. Interfaces*, 2018, **10**, 16768–16775.
27 S. Cordier, F. Grasset, Y. Molard, M. Amela-Cortes, R. Boukherroub, S. Ravaine, M. Mortier, N. Ohashi, N. Saito and H. Haneda, *J. Inorg. Organomet. Polym. Mater.*, 2015, **25**, 189–204.
28 F. A. Cotton, *Inorg. Chem.*, 1964, **3**, 1217–1220.
29 K. Kirakci, P. Kubat, M. Dusek, K. Fejfarova, V. Sicha, J. Mosinger and K. Lang, *Eur. J. Inorg. Chem.*, 2012, 3107–3111.
30 M. A. Mikhaylov and M. N. Sokolov, *Eur. J. Inorg. Chem.*, 2019, 4181–4197.
31 M. N. Sokolov, M. A. Mihailov, E. V. Peresypkina, K. A. Brylev, N. Kitamura and V. P. Fedin, *Dalton Trans.*, 2011, **40**, 6375.
32 Y. Zhao and R. R. Lunt, *Adv. Energy Mater.*, 2013, **3**, 1143–1148.
33 M. Amela-Cortes, Y. Molard, S. Paofai, A. Desert, J.-L. Duvail, N. G. Naumov and S. Cordier, *Dalton Trans.*, 2016, **45**, 237–245.
34 J. Choi, D. Nguyen, E. Gi, K. A. Brylev, J. W. Yu, D. Kim, W. B. Lee, D. H. Kim, I. Chung, K. K. Kim and S.-J. Kim, *J. Mater. Chem. C*, 2022, **10**, 4402–4410.
35 Y. Molard, C. Labbe, J. Cardin and S. Cordier, *Adv. Funct. Mater.*, 2013, **23**, 4821–4825.
36 M. Amela-Cortes, A. Garreau, S. Cordier, E. Faulques, J.-L. Duvail and Y. Molard, *J. Mater. Chem. C*, 2014, **2**, 1545–1552.
37 M. Robin, W. Kuai, M. Amela-Cortes, S. Cordier, Y. Molard, T. Mohammed-Brahim, E. Jacques and M. Harnois, *ACS Appl. Mater. Interfaces*, 2015, **7**, 21975–21984.
38 M. Robin, N. Dumait, M. Amela-Cortes, C. Roiland, M. Harnois, E. Jacques, H. Folliot and Y. Molard, *Chem. – Eur. J.*, 2018, **24**, 4825–4829.
39 K. Kirakci, K. Fejfarova, M. Kucerakova and K. Lang, *Eur. J. Inorg. Chem.*, 2014, 2331–2336.
40 K. Kirakci, M. A. Shestopalov and K. Lang, *Coord. Chem. Rev.*, 2023, **481**, 215048.
41 M. A. Mikhailov, K. A. Brylev, P. A. Abramov, E. Sakuda, S. Akagi, A. Ito, N. Kitamura and M. N. Sokolov, *Inorg. Chem.*, 2016, **55**, 8437–8445.
42 C. Fouquey, J.-M. Lehn and A.-M. Levelut, *Adv. Mater.*, 1990, **2**, 254–257.
43 A. Gooch, N. S. Murphy, N. H. Thomson and A. J. Wilson, *Macromolecules*, 2013, **46**, 9634–9641.
44 R. J. Thibault, T. H. Galow, E. J. Turnberg, M. Gray, P. J. Hotchkiss and V. M. Rotello, *J. Am. Chem. Soc.*, 2002, **124**, 15249–15254.
45 O. Uzun, A. Sanyal, H. Nakade, R. J. Thibault and V. M. Rotello, *J. Am. Chem. Soc.*, 2004, **126**, 14773–14777.
46 H. Xu, T. B. Norsten, O. Uzun, E. Jeoung and V. M. Rotello, *Chem. Commun.*, 2005, 5157–5159.
47 P. Thordarson, *Chem. Soc. Rev.*, 2011, **40**, 1305–1323.
48 C. M. Cheng, M. I. Egbe, J. M. Grasshoff, D. J. Guarrera, R. P. Pai, J. C. Warner and L. D. Taylor, *J. Polym. Sci., Part A: Polym. Chem.*, 1995, **33**, 2515–2519.
49 A. Udagawa, P. Johnston, H. Uekusa, H. Koshima, K. Saito and T. Asahi, *ACS Sustainable Chem. Eng.*, 2016, **4**, 6107–6114.
50 M. Inada, A. Udagawa, S. Sato, T. Asahi and K. Saito, *Photochem. Photobiol. Sci.*, 2022, **21**, 2169–2177.
51 A. A. Avdeenko, T. L. Dobrovolskaya, V. A. Kultchitsky, Y. V. Naboikin and S. N. Pakulov, *J. Lumin.*, 1976, **11**, 331–337.
52 G. Oster, N. Geacintov and A. U. Khan, *Nature*, 1962, **196**, 1089–1090.
53 S. Khlifi, N. Fournier Le Ray, S. Paofai, M. Amela-Cortes, H. Akdas-Kilic, G. Taupier, S. Derien, S. Cordier, M. Achard and Y. Molard, *Mater. Today*, 2020, **35**, 34–41.
54 I. V. Kashnik, B. Yang, S. S. Yarovoi, T. S. Sukhikh, M. Cordier, G. Taupier, K. A. Brylev, P.-A. Bouit and Y. Molard, *Chem. – Eur. J.*, 2024, **30**, e202400079.
55 A. Dirksen, U. Hahn, F. Schwanke, M. Nieger, J. N. H. Reek, F. Vögtle and L. De Cola, *Chem. – Eur. J.*, 2004, **10**, 2036–2047.
56 Y.-X. Wang, Y.-M. Zhang and Y. Liu, *J. Am. Chem. Soc.*, 2015, **137**, 4543–4549.